Geodetic Evidence for Cascading Landslide Motion Triggered by Extreme Rain Events at Joshimath, NW Himalaya

K. M. Sreejith[1] , M. C. M. Jasir[1,2] , P. S. Sunil[3] , M. S. Rose[3] , Ajish P. Saji[4] , R. Agrawal[1] , M. T. Bushair[5], K. Vijay Kumar[4], and N. M. Desai[1]

[1]Space Applications Centre, Indian Space Research Organisation, Ahmadabad, India, [2]Department of Geophysics, Andhra University, Visakhapatnam, India, [3]Department of Marine Geology and Geophysics, Cochin University of Science and Technology, Kochi, India, [4]Indian Institute of Geomagnetism, Department of Science and Technology, Mumbai, India, [5]India Meteorological Department, Ministry of Earth Sciences, New Delhi, India

Abstract Slope instability due to tectonic, hydrological and anthropogenic activities cause severe landslides in Himalaya. Joshimath, a densely populated Himalayan town witnessed a catastrophic landslide event during December 2022 and January 2023 causing damages to ∼700 buildings. We use Interferometric synthetic aperture radar, Global Positioning System and rainfall measurements to probe the kinematics of the Joshimath landslide. We separate the seasonal and episodic deformation components using singular spectrum analysis. While the low amplitude annual landslide motions are modulated by seasonal precipitation, acceleration phases are triggered by extreme rain events. Our analysis revealed episodes of cascading motions triggered by extreme rain events resulting an overall increase in landslide velocity from −22 mm/yr during 2004–2010 to −325 mm/yr during 2022–2023. We estimate the landslide depth (∼30 m) and hydraulic diffusivity ($\sim 3 \times 10^{-5}$ m^2/s) using a 1-D pore-water pressure diffusion model. Our study reveals the importance of systematic monitoring of ground deformation and weather parameters for landslide hazard mitigation.

Plain Language Summary The Himalayas, world's largest and youngest mountain range formed as a result of the India-Eurasia continental collision hosts thousands of landslides each year related to tectonic and anthropogenic activities. It is important to characterize the landslide kinematics, especially the slow moving landslides at the fast-developing Himalayan urban centers for hazard assessment. A recent catastrophic landslide event in the Joshimath town in NW Himalaya occurred between December 2022 and January 2023 caused damages to ∼700 buildings leading to mass evacuation. We map the spatio-temporal evolution of land deformation at Joshimath using about two decades of geodetic measurements and singular spectrum analysis technique. While the decadal-scale landslide motions match well with the overall increase in rainfall intensity, the episodic accelerations are triggered by extreme rain events. The extreme rainfall event on 19 October 2021, triggered the latest episode of landslide acceleration, which eventually led to the tragic disaster. The present study, for the first time, provides constraints on the landslide depth and hydraulic diffusivity. Our study also emphasis on the systematic monitoring of ground deformation and weather parameters at the Himalayas for an effective landslide hazard preparedness and mitigation.

1. Introduction

The entire Himalayan mountain belt, particularly the regions of Lesser and Higher Himalaya, are prone to landslides due to natural (tectonic and hydrological activities) and anthropogenic activities (slope cuttings for roads construction, dam, and reservoir impoundment, etc.). The Himalayan region witnessed several major landslides in the past few decades claiming thousands of lives and collateral damages (e.g., Mey et al., 2023 and references therein). Apart from published papers, extensive database on the landslide inventories and landslide hazard zonation has been regularly prepared and published by Geological Survey of India (SOI) (https://bhukosh.gsi.gov.in/Bhukosh/Public). These inventories are indeed helpful to understand landslide prone zones, but have limited or no information on the geophysical parameters of the landslides such as the velocity, depth and hydraulic diffusivity etc. A recent review of literature suggests that depth of the landslide is unknown for ∼86% of reported landslides from the Indian Himalayan region (Das et al., 2022). Monitoring and modeling of the landslide kinematics help us to understand landslide kinematics and their causative factors. Geodetic monitoring of landslides, particularly slow-moving landslides using Interferometric synthetic aperture radar (InSAR) and Global

Software: M. C. M. Jasir, R. Agrawal
Validation: K. M. Sreejith, M. C. M. Jasir, P. S. Sunil, M. S. Rose, Ajish P. Saji, K. Vijay Kumar
Visualization: K. M. Sreejith, M. C. M. Jasir
Writing – original draft: K. M. Sreejith
Writing – review & editing: M. C. M. Jasir, P. S. Sunil

Positioning System (GPS) has been well-established for past two decades (e.g., Handwerger et al., 2019; Hu et al., 2018; Yadav et al., 2020). However, lack of dense GPS network and loss of InSAR coherence at the steep slopes of the Himalayas imposes a major challenge to characterize the landslide kinematics (e.g., Yadav et al., 2020).

Joshimath, a small town situated south of Dhauliganga River in Chamoli District of Uttarakhand, (NW Himalaya) has a long history of land subsidence for more than three decades (Bhattacharya & Jugran, 1982; Bisht & Rautela, 2010). The latest catastrophic event was reported by the end of 2022 causing ground cracks and damages to more than 700 buildings (Chadha, 2023; Gahalaut et al., 2023; Sati et al., 2023). On 8 January 2023, the region has been officially declared as a landslide and subsidence-hit zone. We map spatio-temporal kinematics of the Joshimath landslide leveraging about two decades of geodetic (InSAR and GPS) and rainfall data sets. The purpose of this study is to examine whether the land deformation at Joshimath is a rapid response to an anthropogenic or natural process or a rapid intensification of a long-term movement. We also attempted to separate the seasonal and episodic deformation components using Singular Spectrum Analysis (SSA) and to characterize the geometrical and hydrological properties of the landslide.

2. Study Area

Earthquakes caused by the strain release related to the India-Eurasia collision system (e.g., Bilham et al., 2001; Sreejith et al., 2016, 2018), high topography with steep slopes, seasonal and intense rainfall events make the NW Himalaya as one of the most vulnerable regions for landslides and slope instability. The Joshimath town is situated north of the Vaikrita Thrust within the Main Central Thrust Zone along a steep slope toward the confluence of the Dhauliganga and Alaknanda rivers (Figures 1a and 1b, Figure S1a in Supporting Information S1). The hill slope is made of highly jointed gneisses with loose landslide material, possibly related to a large-scale paleo-landslide (Mishra, 1976). Field observations and high-resolution satellite imageries revealed several landslide scarps down-slope toward the Dhauliganga River, suggesting slope instability (Figure 1). Our field observations also include partially subsided roads, damaged buildings and en-echelon shaped down-slope land subsidence (Figure 1). Interactions with the local residents revealed that the region had experienced isolated incidents of building collapses and damages for several years due to land subsidence and deformation. However, a series of catastrophic land deformation and building collapse events were reported since December 2022. There are also claims that a dam and tunnel system for hydropower generation under construction by the National Thermal Power Corporation has a role in the Joshimath crisis (Bisht & Rautela, 2010). Nevertheless, this hydropower plant was massively damaged by the huge debris and water flow along the Dhauliganga (Shugar et al., 2021) as a result of the 7 February 2021 glacier-rock avalanche (Figure S1a in Supporting Information S1).

3. Data Sets

3.1. InSAR

SAR images from ALOS-1, Sentinel-1 and ALOS-2 were processed using ISCE software (Rosen et al., 2012) to generate interferogram stacks. ENVISAT data were processed using GMTSAR software (Sandwell et al., 2011). Time-series analysis were carried out using the Small Baseline Subset Interferometry Technique (Berardino et al., 2002) implemented in the MintPy software (Yunjun et al., 2019). Details of SAR data used (Table S1 in Supporting Information S1 and Table S2) and InSAR processing strategies adopted are provided in Supporting Information S1 (Text S1, Figures S2–S7).

3.2. GPS

GPS observations from a permanent and a campaign station located within the Joshimath landslide region (Figure 1) were utilized for the present work. Data from the permanent GPS site, established by SOI, were available from January 2022 to January 2023. Data from the campaign GPS site, established by Indian Institute of Geomagnetism (IIG) in May 2014, were annually collected until 2018 (Saji et al., 2020). After the Joshimath landslide disaster, we re-occupied this station and collected data from 22 to 26 April 2023. GPS data sets were processed using GAMIT/GLOBK software (Herring, 2005; King & Bock, 2005). To understand the state of deformation related to the landslide motion, we derived the residual time-series in Indian Reference Frame by removing the Indian plate Euler pole and angular velocity (Ader et al., 2012). Details of GPS data processing are
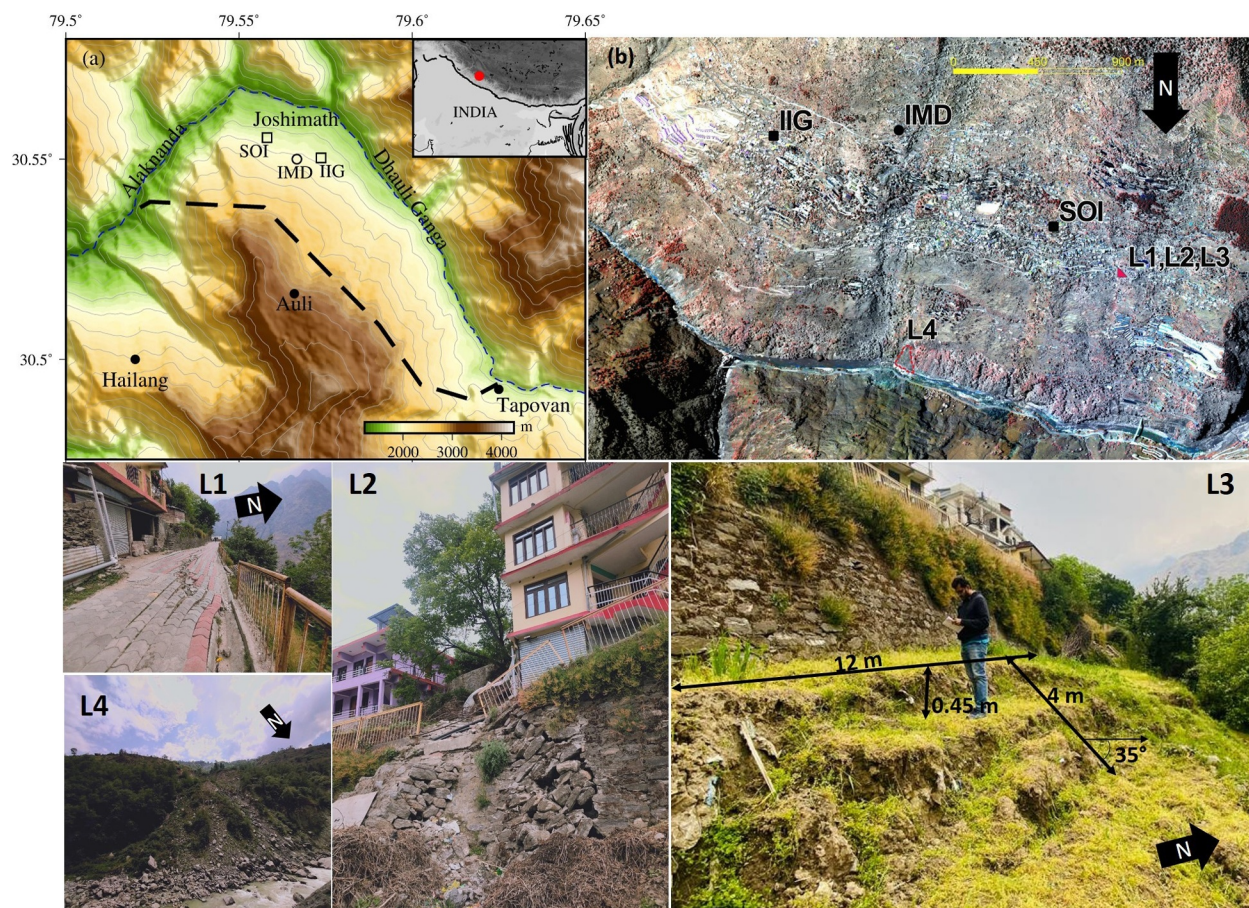
Figure 1. (a) Topography of the Joshimath and surrounding region. Locations of Global Positioning System stations (Survey of India and Indian Institute of Geomagnetism) are marked as open square. Location of the India Meteorological Department weather observatory is marked with an open circle. (b) Satellite imagery (Cartosat 3E) of the Joshimath town. L1, L2, L3, and L4 are locations of field photographs shown in the bottom panels. While L1, L2, and L3 are associated with the 2022–2023 Joshimath disaster, L4 occurred in 2014 at the southern edge of Joshimath.

provided in Text S2 in Supporting Information S1. East, North and Vertical displacement time-series at both the stations are provided in Table S3.

3.3. Rainfall Data

Rainfall data used in the study is from the weather observatory at Joshimath maintained by India Meteorological Department (IMD) located within the Joshimath landslide zone (Figure 1, Figure S1 in Supporting Information S1). Data from the IMD observatory were available from 2021 to 2023 (Table S4). In addition, rain data from other three nearby observatories within the Chamoli district and the merged rainfall products from 2004 to 2021 (Pai et al., 2014) were used for time-series analysis (Text S3 in Supporting Information S1).

4. Analysis and Results

4.1. Landslide Mobility and Rainfall

Maps showing cumulative Line of Sight (LOS) deformation during 2017–2023 derived using Sentinel-1 Ascending (A129) and ALOS-2 Descending (D52) data are presented in Figure 2. The magnitude of deformation along the ascending track (up to −950 mm) is significantly higher compared to the same along the descending track (up to −150 mm), suggesting significant down-slope landslide motion. The permanent GPS station (SOI) situated in the western part of the Joshimath town recorded a displacement of ∼500 mm toward north and ∼ −800 mm in vertical direction during 2022 and 2023 (Figure 2e). The campaign GPS station (IIG) installed in the eastern part of the Joshimath town showed significant horizontal motion of ∼800 mm toward NE direction along
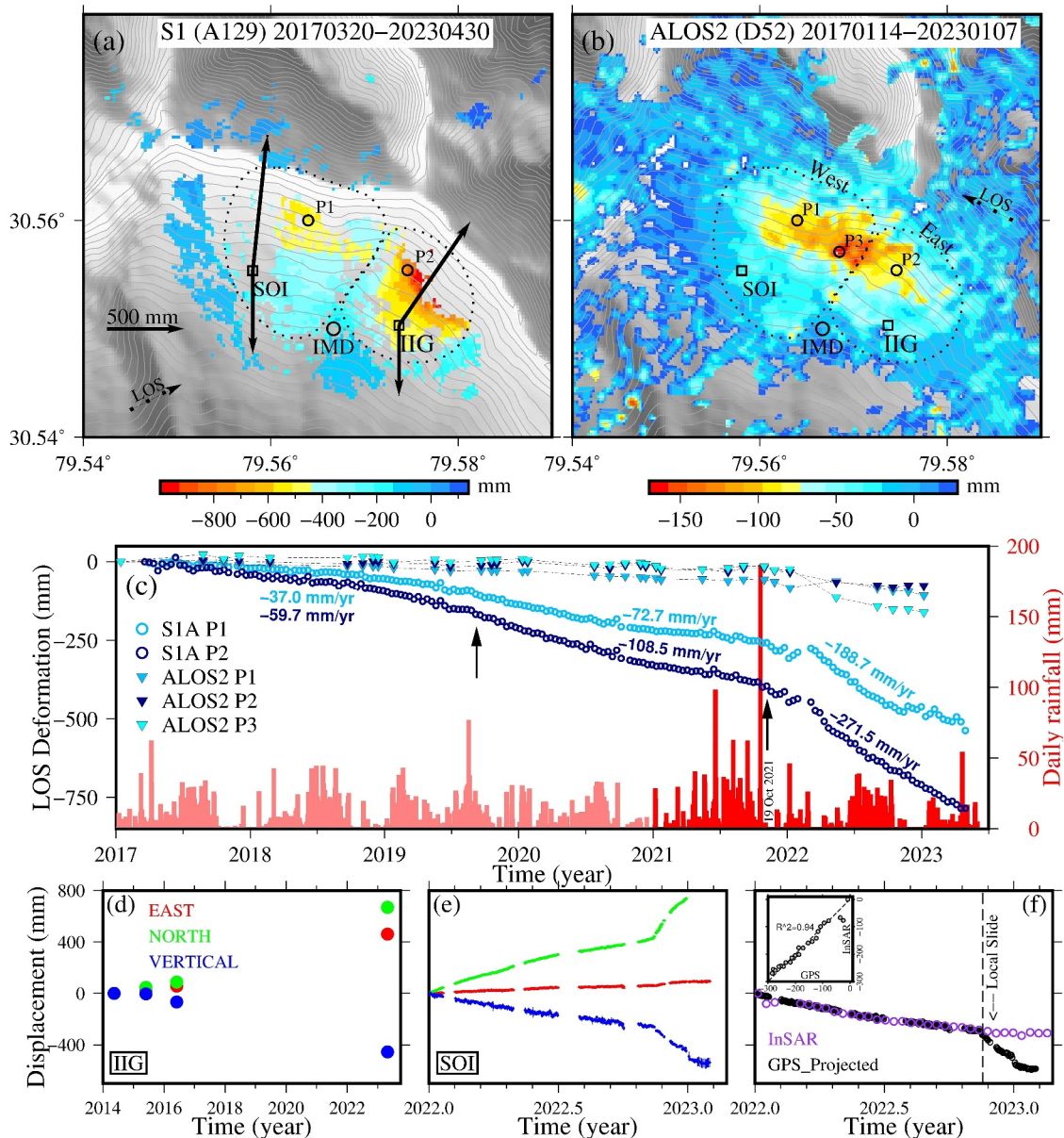
Figure 2. (a) Cumulative Line of Sight (LOS) deformation between 20 March 2017 and 30 April 2023 obtained from time-series analysis of from Sentinel-1 data (Movie S1). Thick black arrows represent horizontal and vertical Global Positioning System (GPS) displacements at stations Indian Institute of Geomagnetism (IIG) (2014–2023) and Survey of India (SOI) (2022–2023). Location of the weather observatory (India Meteorological Department (IMD)) is also shown. P1, P2, and P3 are locations of time series displacements. (b) Cumulative LOS deformation between 14 January 2017 and 7 January 2023 obtained from time-series analysis of from ALOS-2 data (c) Plot showing the time-series LOS displacements at points P1 (light blue), P2 (dark blue) P3 (cyan) and daily rainfall at the IMD station. Rainfall data from gauge-based measurements (2021–2023) and extracted from the merged products (2017–2021) and shown as dark red and light shades, respectively. (d, e) Time-series GPS displacements at IIG and SOI (f) comparison of GPS and Sentinel-1 Interferometric synthetic aperture radar deformation. A dashed line indicates beginning of the local slide at GPS station.

with a subsidence of ~-400 mm during May 2016 and April 2023 (Figure 2d). Thus, considering the overall directions of motion and topographic slope and aspect, the Joshimath landslide could be clearly demarcated to western and eastern segments separated by a roughly NS oriented topographic high (Figures 2a and 2b and Figure S3 in Supporting Information S1). We did not attempt to resolve horizontal (EW, neglecting the NS motion) and vertical deformations as the data clearly suggest significant deformation along the NS direction. As little information is available regarding the nature of the slide (rotational or translational) and its geometry, decomposition of the deformation into 3-D by assuming a parallel basal plane to the surface also will not be realistic.

We use the Sentinel-1 displacement time-series to compare with that derived from the SOI GPS station. As the InSAR pixels co-located with the SOI site were decorrelated, nearest coherent pixel (∼150 m) was used for the comparison (Figure S4a in Supporting Information S1). The InSAR and GPS time series are in good agreement during 5 January 2022 to 1 November 2022 with an average root-mean-square deviation 16.4 mm. However, the rapid-slide between 18 November 2022 and 5 January 2023 (−350 mm, Vertical, 450 mm, NE) recorded in the SOI station is not reflected in the InSAR time series (Figure 2f). This suggests that this rapid slide event is restricted to regions close by the SOI station. Second, localized deformation zones with dimensions <12 m as observed in the field are beyond the InSAR resolution limit (30 m). Similar to our results, Yang et al. (2023) also did not observe notable change in the InSAR time-series during November 2022 and January 2023. Conversely, Shankar et al. (2023) showed comparable results between GPS and Sentinel-1 InSAR (descending) observations. However, we note that the Sentinel-1 descending track at Joshimath has low InSAR sensitivity Index (<0.2) and coherence (<0.4) indicating poor reliability and signal quality, respectively (Figures S3 and S4b in Supporting Information S1). Hence, we primarily rely on Sentinel-1 ascending track due to the favorable acquisition geometry to track the down-slope landslide motion as indicated by a higher radar sensitivity of 0.7–1 (van Natijne et al., 2022).

Time-series InSAR deformation along the ascending track at selected pixels from the western and eastern segments of the Joshimath landslide suggests a non-linear evolution of deformation with similar trends (Figure 2c). LOS deformation clearly depicts systematic increase in landslide motion during 2017–2019 (up to −80 mm/yr), 2019–2022 (up to −150 mm/yr), and 2022–2023 (up to −325 mm/yr) as shown in Figure 2a and Figure S4a in Supporting Information S1. It is interesting to note that these landslide acceleration phases are preceded by extreme rain events (Figure 2c). Following the classification scheme of IMD (IMD, 2021), very heavy (99 percentile) to extremely heavy rainfall events (99.9 percentile) are considered as hazardous and mentioned in the present work as extreme rain events.

In order to further understand the decadal-scale landslide mobility and its relation with the rainfall pattern, we analyzed InSAR and rainfall data during 2004 and 2023 period (Figure 3d and Figures S4–S6 in Supporting Information S1). The annual deformation rates which increased more than 10 times between 2004 and 2023 in episodic and cascading fashion correlate well with the overall increase in the yearly rainfall intensity (yearly rainfall per number of wet days), suggesting a causal relation between them (Figure 3d). At the same time, the rapid changes in the landslide mobility were triggered by extreme rain events (Figure 2c).

4.2. Singular Spectrum Analysis

To understand the nature of landslide mobility and its temporal changes, we applied SSA to decompose the time-series LOS deformation to different components. SSA is a powerful statistical non-parametric technique generally used to identify governing physical phenomena reflected in the geophysical data sets (Vautard et al., 1992; Vautard & Ghil, 1989). We decompose the InSAR data to 30 components and selected the optimum number of eigenvalue as five based on the trade-off curve between the number of components and misfit between the original and reconstructed signal (Figure S8 in Supporting Information S1). Plots showing time-series of five principle components for the western and eastern regions are presented in Figures S9a and S9b in Supporting Information S1, respectively. Details of SSA analysis are provided in Text S4 in Supporting Information S1.

SSA analysis suggests that the observed deformation time-series consists of episodic and periodic components (Figures 4a–4c). The episodic component is dominated by the cascading landslide motion (PC-1) followed by signals (PC-2 and 3) that correlate with the extreme rain events (Figures 4a–4c and Figure S9 in Supporting Information S1). We interpret these signals as landslide accelerations (PC-1) imposed by sudden hydrologic changes (PC-2 and 3) triggered by extreme rain events. This is evident from the large magnitude signal associated with the extreme rain event of 19 October 2021 (Figures 4b and 4c). The SSA analysis also reveals low amplitude periodic deformation that correlate well with the monthly average rainfall data suggesting modulation of landslide motion by the seasonal monsoon rains (Figures 4c and 4e).

4.3. Pore-Water Pressure Diffusion Model

Rainwater infiltration increases pore-water pressure causing landslide acceleration by reducing the Coulomb frictional strength of the landslide material. We use a one-dimensional pore-water pressure model (Cohen-Waeber et al., 2018; Handwerger et al., 2019; Kang et al., 2021) to understand the interactions between rainfall
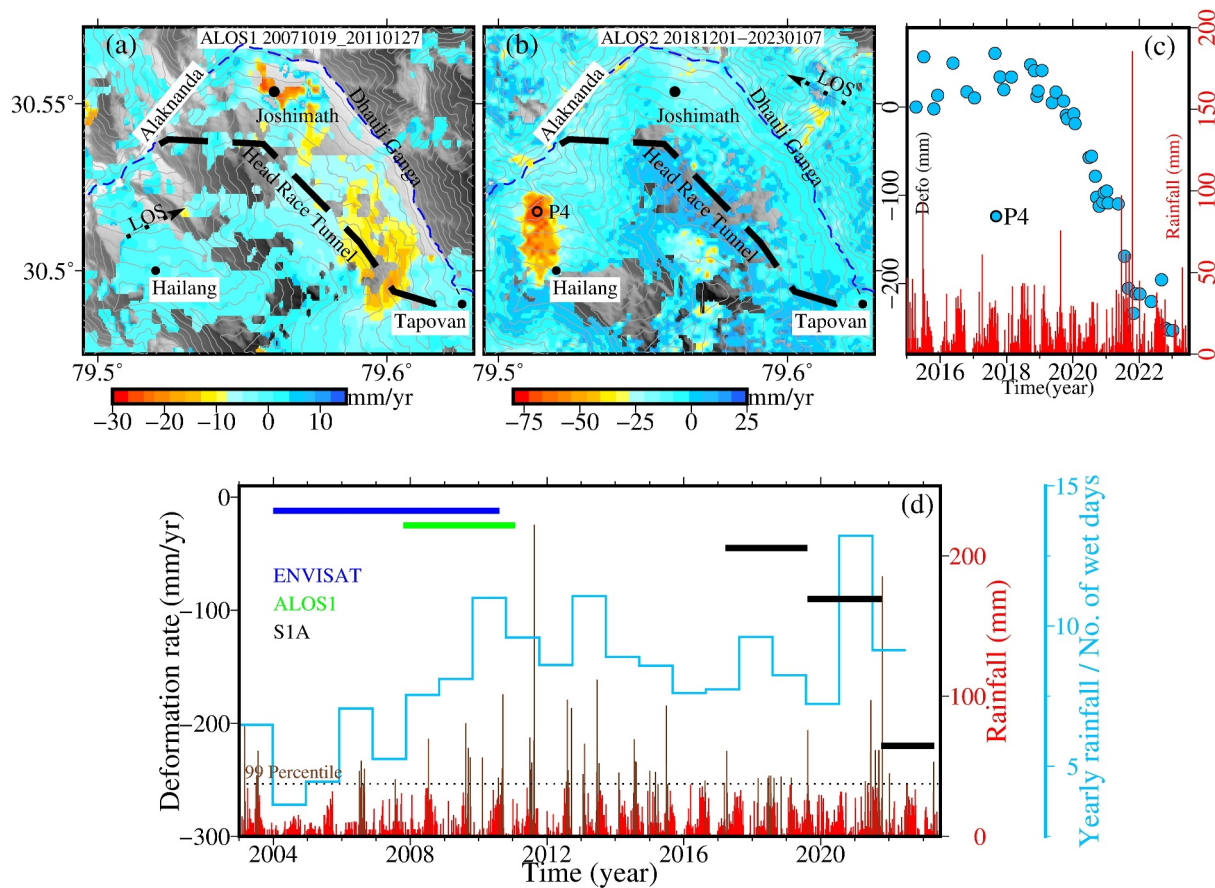
Figure 3. (a) Mean Line of Sight (LOS) deformation rate obtained by linear fit to the ALOS-1 Interferometric synthetic aperture radar (InSAR) time series during 19 October 2007 and 27 January 2011. (b, c) Mean LOS deformation rate obtained by linear fit to the ALOS-2 InSAR time series during 1 December 2018 and 7 January 2023 and time-series deformation at P4 (d) Mean deformation rate obtained from ENVISAT, ALOS-1, and Sentinel-1 InSAR analysis and annual variations in rainfall intensity during 2004 and 2023 (light blue lines). Daily rainfall (red) and extreme-events (brown) are also shown.

and landslide motion (Figure 4d). Ideally, ground based observations of pore-water pressure is required to determine effective hydraulic diffusivity (e.g., Kang et al., 2021). Hu et al. (2019) proposed that in the absence of ground based measurements, normalized modeled pore-water pressure and landslide velocity could be used to evaluate the relative changes. Similar to this approach, we used the best-fit cross-correlation between the normalized pore pressure changes at depth and SSA-derived seasonal component of landslide motion to constrain the landslide depth (z) and effective hydraulic diffusivity (D) of the landslide body (Text S5, Figure S10 in Supporting Information S1). We explore a wide range of depths (20–60 m) as estimated from the area-depth scaling relationships (Handwerger et al., 2021; Hu et al., 2019; Larsen et al., 2010) and hydraulic diffusivity (10^{-6} to 10^{-4} m²/s) to test the trade of between them in the pore-water pressure model (Text S5 in Supporting Information S1). The model suggests similar ranges of depth and hydraulic diffusivity for the western ($z = 31$–36 m, $D = 2.85$–3.75×10^{-5} m²/s) and eastern ($z = 25$–29 m, $D = 2.61$–3.3×10^{-5} m²/s) segments (Text S5, Figure S10 in Supporting Information S1). The model estimated landslide depth is well within the range basement depths (25–40 m) reported from recent geophysical field investigations (NGRI, 2023). Model runs by fixing these end-member depths also provide diffusivity ranges (2–4.5×10^{-5} m²/s) similar to that of the grid search method (Figure S10c in Supporting Information S1).

5. Discussion

5.1. Kinematics of Joshimath Landslide and Implications

Our analysis reveals that the episodic accelerations of the Joshimath landslide are triggered by extreme rain events. However, Yang et al. (2023) suggested that the 4.7 magnitude earthquake that occurred on 11 September
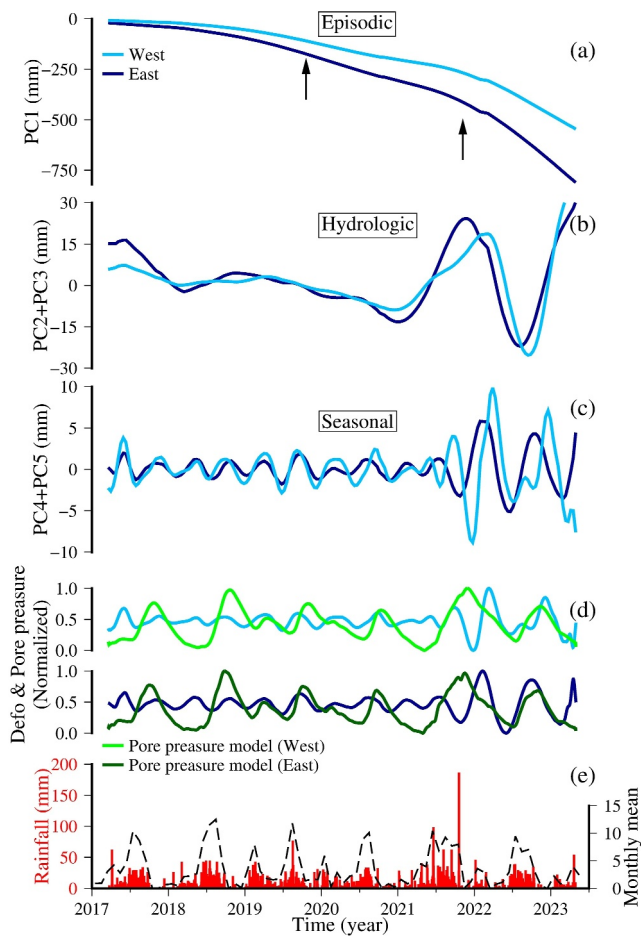
Figure 4. Results of singular spectrum analysis and pore-pressure modeling. (a–c) Episodic, Hydrologic, and Seasonal and component of Line of Sight deformation for the western (light blue) and eastern (dark blue) regions. (d) Correlation between the normalized seasonal component of deformation and the best-fit pore-pressure model. (e) Daily (red histograms) and monthly averaged rainfall data.

2021 could have triggered the landslide acceleration since December 2021. We note that the reported earthquake epicenter is about 28 km away from the Joshimath town and there are no significant earthquakes ($M > 5$) within 30 km for the past 20 years that correlate with the previous episodes of landslide acceleration (Figures 2c and 3d and Figure S1a in Supporting Information S1). Hence, it is difficult to reconcile the role of earthquakes in the mobility of Joshimath landslide. Nevertheless, it is well established that majority of landslides in the NW Himalaya are primarily triggered by rainfall (e.g., Kanungo & Sharma, 2014).

Triggering of landslide acceleration by extreme rain events needs particular attention. On 19 October 2021, the weather station at Joshimath recorded 185 mm rain in 24 hr. This event caused an anomalous deformation component, two-fold increase in the amplitude of the seasonal deformation, followed by a two-fold increase in landslide velocity that finally culminated to the 2022 Joshimath disaster (Figures 2c, 4b, and 4c). The catastrophic landslide motion associated with this event appears to be widespread, yet highly localized without causing a collapse to the entire landslide body as observed in the field. Second, a large-scale collapse would have caused morphological changes, particularly toward the landslide toe, due to the prominent down-slope motion. However, no visible changes in the landform, including local slides associated with the 2022 disaster, were observed at the exposed toe abutting the Dhauliganga River.

The Joshimath landslide area could be divided into western and eastern segments with distinct topographic characteristics and direction of movements that follows the paleo-landslide deposit trend (Sati et al., 2023; Sundriyal et al., 2023). However, similar temporal evolution of deformation, depth, hydraulic diffusivity suggest that the landslide motion would have been controlled by the same processes for both the segments. The difference in magnitude of the motion could be related to hydrological and/or geomorphic characteristics (Figure S3 in Supporting Information S1). It is important to note that building collapse and other catastrophic events are reported from areas of moderate landslide motion in the fast-developing western segment (Figure 1). Sustainable development with implementation of safe construction practices are important for Joshimath and other Himalayan towns.

Another important aspect regarding the Joshimath landslide is the influence of anthropogenic activities. As a part of the Tapovan hydro-power project, a tunnel is being excavated since 2006 from Tapovan to Helong village (Naithani & Murthy, 2006). The location of this headrace tunnel is about 13 km south of the Joshimath town (Figures 1a, 3a, and 3b). On 24 December 2009, the tunnel-boring machine punctured the water-bearing strata causing a water discharge of 700–800 litters/second for more than a month (Bisht & Rautela, 2010). ALOS-1 InSAR data between 2007 and 2011 suggest −15 to −20 mm/yr surface deformation close to the tunnel location (Figure 3a). This could be a manifestation of the ground subsidence related to the large-scale tunneling activities (Sati et al., 2023). However, ALOS-2 InSAR analysis between 2015 and 2023 did not suggest significant deformation in this area (Figure 3b). This indicates that the tunneling process would have caused a localized deformation for a shorter period and may not have caused direct impact on the Joshimath landslide mobility. Indeed, the changes in hydro-geological setup due to tunneling and urbanization could have a significant impact on the slope stability (Dille et al., 2020).

5.2. Landslide Mechanism

The mechanism of long-term landslide motion triggered by extreme events at Joshimath is an interesting aspect. The landslide accelerations are triggered by a sudden change in pore-pressure and further controlled/maintained by the rate and state frictional properties of the materials coupled with the pore-pressure feedbacks (Lacroix

et al., 2020 and references therein). Rate-strengthening friction and/or decrease in pore-pressure can stabilize these accelerated motions over a period of time (Handwerger et al., 2016). However, relatively long-spells of accelerated but stable sliding of the Joshimath landslide implies a rate-weakening mechanism. Numerical models also suggests that the slow moving landslides within velocity-weakening medium could creep in decadal-scale before transitioning to runaway failure (Paul et al., 2024). Lack of long lasted dry-spells between episodes of accelerated phases (Figure 2) would have also played a role in maintaining the stable motion of the Joshimath landslide. Nevertheless, over seasonal time scales, the landslide response to rise in pore-water pressure is more prominent than that of decrease in pore-water pressure (Carey et al., 2019).

5.3. Landslide Depth and Hydraulic Diffusivity

Our one dimensional pore-water pressure diffusion model provided first order constraints to the depth and hydraulic diffusivity of the Joshimath landslide. The hydraulic diffusivity of Joshimath slide appears to be well within the range of 10^{-4} to 10^{-6} m^2/s reported for deep seated, slow moving landslides elsewhere (Handwerger et al., 2019; Hu et al., 2019; Kang et al., 2021). However, in order to understand the interaction of in-filtered water at depth and its influence on the frictional properties of the failure surface and hence the landslide kinematics (Finnegan et al., 2021; Handwerger et al., 2013; Iverson, 2000, 2005; Schulz et al., 2009), detailed geophysical/geotechnical experiments need to be carried out.

5.4. Detection of a New Landslide Zone

The ALOS-2 InSAR analysis revealed a ~3.5 km^2 deformation zone near Hailang village, toward ~6 km southwest of Joshimath town. This deformation zone is aligned along a sloppy deforested farmland with maximum deformation near the toe (Figure 3b). Considering the topography, orientation, the deformation zones and satellite look direction, the land movements recorded by the ALOS-2 at Hailang could be related to a slow moving landslide. Time-series InSAR data clearly suggests the inception of the Hailang landslide after mid-2018 (Figure 3c). It is important to note that the deformation rate at Hailang (up to −75 mm/yr) is similar to that of Joshimath between 2017 and 2019, but did not show episodic acceleration in response to extreme rain events (Figure 3c). The landslide would have been caused by slope-instability imposed by hydrological imbalance. Systematic geodetic observations from the upcoming NASA-ISRO Synthetic Aperture Radar mission will have a major role in monitoring such catastrophic landslides.

6. Conclusions

Joint analysis of InSAR, GPS and rainfall data revealed constraints on the spatio-temporal mobility of Joshimath landslide. Major conclusions of the study are:

1. Kinematics of Joshimath landslide includes both episodic accelerations and seasonal motions. Low amplitude annual landslide motion is modulated by seasonal precipitation whereas, the episodic accelerations are triggered by extreme rain events.
2. Our analysis revealed several episodes of cascading motions triggered by extreme rain events resulting an overall increase in landslide velocity from ~−22 mm/yr during 2004–2010 upto ~−325 mm/yr during 2022–2023 culminating in to the series of catastrophic land deformation events occurred between December 2022 and January 2023.
3. 1-D pore-pressure diffusion model provided first order constraints on the depth (~30 m) and hydraulic diffusivity (~3 × 10^{-5} m^2/s) of the Joshimath landslide.
4. Our InSAR analysis detects another active landslide 6 km SW of the Joshimath town that has been moving with a velocity of ~−75 mm/yr since mid-2018.
5. The present study warrants systematic observations of ground deformation and meteorological parameters at the Himalayas for landslide hazard mitigation.

Data Availability Statement

SAR data from Sentinel-1 and ALOS-1 satellites are available from Alaska Satellite Facility (https://search.asf.alaska.edu/#/). ALOS-2 data, provided by JAXA through RA-6, PI No. 3053 and EOR3A2N140, are available at https://gportal.jaxa.jp/gpr, could be accessed after user registration (https://gportal.jaxa.jp/gpr/user/regist1?

lang=en). ENVISAT ASAR data are available at European Space Agency (2016) (https://earth.esa.int/eogate-way/catalog/envisat-asar-im-l0-asa_im__0p-?text=envisat+asar+im+l0+%5Basa_im__0p%5D). Shuttle Radar Topography Mission (SRTM) data (Farr et al., 2007; NASA JPL, 2013) was retrieved from (https://step.esa.int/auxdata/dem/SRTMGL1/). Gridded/merged rainfall data (Pai et al., 2014) is available at https://www.imdpune.gov.in/cmpg/Griddata/Rainfall_25_Bin.html. GPS and Rainfall observations at Joshimath are provided in Tables S3 and S4, respectively. All software used in this work are openly available: MintPy (https://github.com/insarlab/MintPy); ISCE2 (https://github.com/isce-framework/isce2); GMTSAR (https://github.com/gmtsar/gmtsar); GAMIT/GLOBK (http://geoweb.mit.edu/gg/); GMT (https://github.com/GenericMappingTools). Code used for SSA analysis is available at https://github.com/anton-a-tkachev/SSA-for-Matlab.

References

Ader, T., Avouac, J.-P., Liu-Zeng, J., Lyon-Caen, H., Bollinger, L., Galetzka, J., et al. (2012). Convergence rate across the Nepal himalaya and interseismic coupling on the Main Himalayan Thrust: Implications for seismic hazard. *Journal of Geophysical Research*, 117(B4), B04403. https://doi.org/10.1029/2011JB009071

Berardino, P., Fornaro, G., Lanari, R., & Sansosti, E. (2002). A new algorithm for surface deformation monitoring based on small baseline differential SAR interferograms. *IEEE Transactions on Geoscience and Remote Sensing*, 40(11), 2375–2383. https://doi.org/10.1109/TGRS.2002.803792

Bhattacharya, A., & Jugran, D. K. (1982). Landslide due to mass sinking phenomenon: Sunil-Joshimath of U.P. Himalaya example. *Journal of the Indian Society of Photo-interpretation and Remote Sensing*, 10(1), 53–55. https://doi.org/10.1007/bf02990706

Bilham, R., Gaur, V. K., & Molnar, P. (2001). Himalayan seismic hazard. *Science*, 293(5534), 1442–1444. https://doi.org/10.1126/science.1062584

Bisht, M. P. S., & Rautela, P. (2010). Disaster looms large over Joshimath town. *Current Science*, 98, 1271.

Carey, J. M., Massey, C. I., Lyndsell, B., & Petley, D. N. (2019). Displacement mechanisms of slow-moving landslides in response to changes in porewater pressure and dynamic stress. *Earth Surface Dynamics*, 7(3), 707–722. https://doi.org/10.5194/esurf-7-707-2019

Chadha, R. K. (2023). 2022 Joshimath subsidence. *Journal of the Geological Society of India*, 99(2), 289. https://doi.org/10.1007/s12594-023-2298-9

Cohen-Waeber, J., Bürgmann, R., Chaussard, E., Giannico, C., & Ferretti, A. (2018). Spatiotemporal patterns of precipitation-modulated landslide deformation from independent component analysis of InSAR time series. *Geophysical Research Letters*, 45(4), 1878–1887. https://doi.org/10.1002/2017GL075950

Das, S., Sarkar, S., & Kanungo, D. P. (2022). A critical review on landslide susceptibility zonation: Recent trends, techniques, and practices in Indian Himalaya. *Natural Hazards*, 115(1), 23–72. https://doi.org/10.1007/s11069-022-05554-x

Dille, A. O., Dewitte, A. L., Handwerger, N., d'Oreye, D., Ganza Bamulezi, G. G. G., Bamulezi, G. I., et al. (2020). Acceleration of a large deep-seated tropical landslide due to urbanization feedbacks. *Nature Geoscience*, 15(12), 1048–1055. https://doi.org/10.1038/s41561-022-01073-3

European Space Agency. (2016). Envisat ASAR image mode L0 product [Dataset]. *IPF Version 6.03*. https://doi.org/10.5270/EN1-q74d24h

Farr, T. G., Rosen, P. A., Caro, E., Crippen, R., Duren, R., Hensley, S., et al. (2007). The shuttle radar topography mission. *Reviews of Geophysics*, 45(2), RG2004. https://doi.org/10.1029/2005RG000183

Finnegan, N. J., Perkins, J. P., Nereson, A. L., & Handwerger, A. L. (2021). Unsaturated flow processes and the onset of seasonal deformation in slow-moving landslides. *Journal of Geophysical Research: Earth Surface*, 126(5), e2020JF005758. https://doi.org/10.1029/2020JF005758

Gahalaut, V. K., Gurjar, N., Kumar, A., Rajewar, S., Mohanty, A., Kumar, A., et al. (2023). Creeping slopes in NW Himalaya and Joshimath slide: Constraints from GPS measurements. *Geomatics, Natural Hazards and Risk*, 14(1), 2263622. https://doi.org/10.1080/19475705.2023.2263622

Handwerger, A. L., Booth, A. M., Huang, M. H., & Fielding, E. J. (2021). Inferring the subsurface geometry and strength of slow-moving landslides using 3-D velocity measurements from the NASA/JPL UAVSAR. *Journal of Geophysical Research: Earth Surface*, 126(3), e2020JF005898. https://doi.org/10.1029/2020JF005898

Handwerger, A. L., Huang, M.-H., Fielding, E. J., Booth, A. M., & Bürgmann, R. (2019). A shift from drought to extreme rainfall drives a stable landslide to catastrophic failure. *Scientific Reports*, 9(1), 1569. https://doi.org/10.1038/s41598-018-38300-0

Handwerger, A. L., Rempel, A. W., Skarbek, R. M., Roering, J. J., & Hilley, G. E. (2016). Rate-weakening friction characterizes both slow sliding and catastrophic failure of landslides. *Proceedings of the National Academy of Sciences*, 113(37), 10281–10286. https://doi.org/10.1073/pnas.1607009113

Handwerger, A. L., Roering, J. J., & Schmidt, D. A. (2013). Controls on the seasonal deformation of slow-moving landslides. *Earth and Planetary Science Letters*, 377(378), 239–247. https://doi.org/10.1016/j.epsl.2013.06.047

Herring, T. A. (2005). GLOBK, Global Kalman filter VLBI and GPS analysis program, version 10.2, report, Department of Earth, Atmospheric and Planetary Sciences, Massachussetts Institute of Technology.

Hu, X., Bürgmann, R., Lu, Z., Handwerger, A. L., Wang, T., & Miao, R. (2019). Mobility, thickness, and hydraulic diffusivity of the slow-moving Monroe landslide in California revealed by L-band satellite radar interferometry. *Journal of Geophysical Research: Solid Earth*, 124(7), 7504–7518. https://doi.org/10.1029/2019JB017560

Hu, X., Lu, Z., Pierson, T. C., Kramer, R., & George, D. L. (2018). Combining InSAR and GPS to determine transient movement and thickness of a seasonally active low-gradient translational landslide. *Geophysical Research Letters*, 45(3), 1453–1462. https://doi.org/10.1002/2017GL076623

India Meteorological Department. (2021). *Standard operation procedure-weather forecasting and warning, Ministry of Earth Sciences*. Government of India. Retrieved from https://mausam.imd.gov.in/imd_latest/contents/pdf/forecasting_sop.pdf

Iverson, R. M. (2000). Landslide triggering by rainfall infiltration. *Water Resources Research*, 36(7), 1897–1910. https://doi.org/10.1029/2000wr900090

Iverson, R. M. (2005). Regulation of landslide motion by dilatancy and pore pressure feedback. *Journal of Geophysical Research*, 110(F2), F02015. https://doi.org/10.1029/2004JF000268

Kang, Y., Lu, Z., Zhao, C., Xu, Y., Kim, J., & Gallegos, A. J. (2021). InSAR monitoring of creeping landslides in mountainous regions: A case study in Eldorado National forest, California. *Remote Sensing of Environment*, 258, 112400. https://doi.org/10.1016/j.rse.2021.112400

Kanungo, D. P., & Sharma, S. (2014). Rainfall thresholds for prediction of shallow landslidesaround Chamoli-Joshimath region, Garhwal Himalayas. *Landslides*, *11*(4), 629–638. https://doi.org/10.1007/s10346-013-0438-9

King, R. W., & Bock, Y. (2005). *Documentation for the GAMIT GPS processing software release 10.2*. Massachusetts Institute of Technology.

Lacroix, P., Handwerger, A. L., & Bièvre, G. (2020). Life and death of slow-moving landslides. *Nature Reviews Earth & Environment*, *1*(8), 404–419. https://doi.org/10.1038/s43017-020-0072-8

Larsen, I. J., Montgomery, D. R., & Korup, O. (2010). Landslide erosion controlled by hillslope material. *Nature Geoscience*, *3*(4), 247–251. https://doi.org/10.1038/ngeo776

Mey, J., Guntu, R. K., Plakias, A., de Almeida, I. S., & Schwanghart, W. (2023). More than one landslide per road kilometer–surveying and modelling mass movements along the Rishikesh-Joshimath (NH-7) highway, Uttarakhand, India. *Natural Hazards and Earth System Sciences*. https://doi.org/10.5194/nhess-2022-295

Mishra, M. C. (1976). *Committees report on sinking of Joshimath*. Government.

Naithani, A. K., & Murthy, K. S. K. (2006). Geological and geotechnical investigations of Tapovan–Vishnugad Hydroelectric project, Chamoli district, Uttarakhand, India. *Journal of Nepal Geological Society*, *34*, 1–16. https://doi.org/10.3126/jngs.v34i0.31873

NASA, J. P. L. (2013). NASA shuttle radar topography mission Global 1 arc second [Dataset]. *NASA EOSDIS Land Processes DAAC*. https://doi.org/10.5066/F7K072R7

National Geophysical Research Institute (NGRI). (2023). Geological & geotechnical studies to understand shallow subsurface strata at Joshimath, Chamoli, Uttarakhand,Technical report. No.: NGRI-2023-SEISM-1018. Retrieved from https://usdma.uk.gov.in/IEC/josimath-reports-1395.aspx

Pai, D. S., Sridhar, L., Rajeevan, M., Sreejith, O. P., Satbhai, N. S., & Mukhopadhyay, B. (2014). Development of a new high spatial resolution (0.25° × 0.25°) long period (1901–2010) daily gridded rainfall data set over India and its comparison with existing data sets over the Region. *Mausam*, *65*, 1–18. https://doi.org/10.54302/mausam.v65i1.851

Paul, K., Bhattacharya, P., & Misra, S. (2024). Frictional control on accelerating creep during the slow-to-fast transition of rainfall-induced catastrophic landslides. *Journal of Geophysical Research: Earth Surface*, *129*(1), e2023JF007213. https://doi.org/10.1029/2023JF007213

Rosen, P. A., Gurrola, E., Sacco, G. F., & Zebker, H. (2012). The InSAR scientific computing environment. In *EUSAR 2012; 9th European conference on synthetic aperture radar* (pp. 730–733).

Saji, A. P., Sunil, P. S., Sreejith, K. M., Gautam, P. K., Kumar, K. V., Ponraj, M., et al. (2020). Surface deformation and influence of hydrological mass over Himalaya and North India revealed from a decade of continuous GPS and GRACE observations. *Journal of Geophysical Research: Earth Surface*, *125*(1), e2018JF004943. https://doi.org/10.1029/2018JF004943

Sandwell, D., Mellors, R., Tong, X., Wei, M., & Wessel, P. (2011). Open radar interferometry software for mapping surface deformation. *EOS. Transaction American Geophysical Union*, *92*(28), 234. https://doi.org/10.1029/2011EO280002

Sati, S. P., Asim, M., Sundriyal, Y. P., Rana, N., Bahuguna, V., & Sharma, S. (2023). Unstable slopes and threatened livelihoods of the historical Joshimath town, Uttarakhand Himalaya, India. *Current Science*, *124*(12), 1384–1392.

Schulz, W. H., Kean, J. W., & Wang, G. (2009). Landslide movement in southwest Colorado triggered by atmospheric tides. *Nature Geoscience*, *2*(12), 863–866. https://doi.org/10.1038/ngeo659

Shankar, H., Chauhan, P., Singh, D., Bhandari, R., Bhatt, C. M., Roy, A., et al. (2023). Multi-temporal InSAR and Sentinel-1 for assessing land surface movement of Joshimath town, India. *Geomatics, Natural Hazards and Risk*, *14*(1), 2253972. https://doi.org/10.1080/19475705.2023.2253972

Shugar, D. H., Jackuemart, M., Shean, D., Bhushan, S., Upadhyay, K., Sattar, A., et al. (2021). A massive rock and ice avalanche caused the 2021 disaster at Chamoli, Indian Himalaya. *Science*, *373*(6552), 300–306. https://doi.org/10.1126/science.abh4455

Sreejith, K. M., Sunil, P. S., Agrawal, R., Saji, A. P., Ramesh, D. S., & Rajawat, A. S. (2016). Coseismic and early postseismic deformation due to the 25 April 2015, Mw 7.8 Gorkha, Nepal, earthquake from InSAR and GPS measurements. *Geophysical Research Letters*, *43*(7), 3160–3168. https://doi.org/10.1002/2016GL067907

Sreejith, K. M., Sunil, P. S., Agrawal, R., Saji, A. P., Ramesh, D. S., & Rajawat, A. S. (2018). Audit of stored strain energy and extent of future earthquake rupture in central Himalaya. *Scientific Reports*, *8*(1), 16697. https://doi.org/10.1038/s41598-018-35025-y

Sundriyal, Y., Kumar, V., Chauhan, N., Kaushik, S., Ranjan, R., & Punia, M. K. (2023). Brief communication on the NW Himalayan towns; slipping towards potential disaster. *Natural Hazards and Earth System Science*. https://doi.org/10.5194/nhess-2022-296

van Natijne, A. L., Bogaard, T. A., van Leijen, F. J., Hanssen, R. F., & Lindenbergh, R. C. (2022). A World-wide InSAR sensitivity index for landslide deformation tracking. *International Journal of Applied Earth Observation and Geoinformation*, *111*(2022), 102829. https://doi.org/10.1016/j.jag.2022.102829

Vautard, R., & Ghil, M. (1989). Singular spectrum analysis in nonlinear dynamics, with applications to paleoclimatic time series. *Physica D*, *35*(3), 395–424. https://doi.org/10.1016/0167-2789(89)90077-8

Vautard, R., Yiou, P., & Ghil, M. (1992). Singular-spectrum analysis: A toolkit for short, noisy chaotic signals. *Physica D*, *58*(1–4), 95–126. https://doi.org/10.1016/0167-2789(92)90103-t

Yadav, R. K., Gahalout, V. K., Gautam, P. K., Jayangondaperumal, R., Sreejith, K. M., Singh, I., et al. (2020). Geodetic monitoring of landslide movement at two sites in the Garhwal Himalaya. *Himalayan Geology*, *41*, 21–30.

Yang, F., An, Y., Ren, C., Xu, J., Li, J., Li, D., & Peng, Z. (2023). Monitoring and analysis of surface deformation in alpine valley areas based on multidimensional InSAR technology. *Scientific Reports*, *13*(1), 12896. https://doi.org/10.1038/s41598-023-39677-3

Yunjun, Z., Fattahi, H., & Amelung, F. (2019). Small baseline InSAR time series analysis: Unwrapping error correction and noise reduction. *Computers & Geosciences*, *133*, 104331. https://doi.org/10.1016/j.cageo.2019.104331

References From the Supporting Information

Chen, C. W., & Zebker, H. A. (2001). Two-dimensional phase unwrapping with use of statistical models for cost functions in nonlinear optimization. *Journal of Optical Society of America*, *18*(2), 338–351. https://doi.org/10.1364/JOSAA.18.000338

European Space Agency. (2021). Copernicus Global digital elevation model [Dataset]. *Distributed by Open Topography*. https://doi.org/10.5069/G9028PQB

Fattahi, H., & Amelung, F. (2013). DEM error correction in InSAR time series. *IEEE Transactions on Geoscience and Remote Sensing*, *51*(7), 4249–4259. https://doi.org/10.1109/tgrs.2012.2227761

Mukul, M., Srivastava, V., Jade, S., & Mukul, M. (2017). Uncertainties in the shuttle radar topography mission (SRTM) heights: Insights from the Indian Himalaya and Peninsula. *Scientific Reports*, *7*(1), 41672. https://doi.org/10.1038/srep41672

Vaka, D. S., Kumar, V., Rao, Y., & Deo, R. (2019). Comparison of various DEMs for height accuracy assessment over different terrains of India. In *IGARSS 2019–2019 IEEE International Geoscience and Remote sensing Symposium* (pp. 1998–2001). https://doi.org/10.1109/IGARSS.2019.8898492

Yu, C., Penna, N. T., & Li, Z. (2017a). Generation of real-time mode high-resolution water vapor fields from GPS observations. *Journal of Geophysical Research: Atmospheres*, *122*(3), 2008–2025. https://doi.org/10.1002/2016jd025753

Yu, C., Li, Z., & Penna, N. T. (2017b). Interferometric synthetic aperture radar atmospheric correction using a GPS-based iterative tropospheric decomposition model. *Remote Sensing of Environment*, *204*, 109–121. https://doi.org/10.1016/j.rse.2017.10.038